Phase-jump instability in the bidirectional ring laser with backscattering

T. H. Chyba
Department of Physics and Astronomy, University of Rochester, Rochester, New York 14627
(Received 2 June 1989)

The third-order equations of motion for a bidirectional, inhomogeneously broadened ring laser at line center with backscattering are solved exactly when the additive noise terms are negligible. The resulting solution for the relative phase of the two propagating modes may exhibit steady-state or transient oscillations. For certain initial conditions, the solution is not unique and is unstable. This gives rise to deterministic phase jumps in both the transient and steady-state behavior. A series of phase jumps occurs if the system repeatedly crosses its unstable boundary. These series may be random or periodic if the system is driven by a stochastic or deterministic source, respectively. In all cases, the jumps are multiples of π radians in magnitude. The solution for the intensities provides a means to determine the pump parameter and backscattering coefficients for the laser through intensity measurements, provided the effects of spontaneous emission are negligible. The results are compared with numerical solutions of the original Langevin equations and with experiments.

I. INTRODUCTION

Sudden phase jumps associated with anticorrelated intensity oscillations have recently been predicted[1-4] and observed[4-6] in a remarkably wide variety of ring-laser systems. An unusual feature of these jumps is that they occur in multiples of π radians. We first summarize the models and systems in which these phase jumps appear.

One approach[2,7,8] for a bidirectional laser starts with the semiclassical Maxwell-Bloch equations for a homogeneously broadened gain medium under the uniform field and slowly varying amplitude approximations. The polarization is adiabatically eliminated, the population inversion is expanded in harmonics, and the final seven differential equations of motion arise from the truncation of this expansion. Phase jumps and intensity oscillations are predicted by this model for parameters appropriate for solid-state lasers[3] and CO_2 lasers with nonzero detuning.[2] The anticorrelated intensity oscillations have been observed.[9,10]

Unidirectional and bidirectional far-infrared (FIR) ring lasers for which neither the atomic population nor polarization can be eliminated also exhibit this phase and intensity behavior.[5,6] It has been proposed that the unidirectional FIR laser should exhibit Lorenz-type chaos[11] due to the equivalence[12] between the Lorenz equations and the Maxwell-Bloch equations for a single-mode homogeneously broadened ring laser. Experiments at high gas pressure confirm this, although those at lower gas pressures reveal more complicated dynamics.[5,13] In both cases, sudden π jumps in phase are observed.[5] The bidirectional FIR laser also exhibits similar phase and intensity behavior when operated at high pressures.[6]

Phase jumps and intensity oscillations are predicted in a related deterministic model which also retains the atomic polarization in the Maxwell-Bloch equations, but assumes a multimode, unidirectional ring cavity whose inversion is sinusoidally modulated.[1]

We have recently reported[4] theoretical predictions and experimental observations of such π phase jumps and intensity oscillations in an inhomogeneously broadened bidirectional ring laser described by the usual third-order Langevin equations without detuning, provided complex terms representing the effects of backscattering from one mode into the other are added.[4,14-27] In contrast with the preceding models, these equations include stochastic noise terms representing spontaneous emission and have both the atomic polarization and inversion adiabatically eliminated from them. This model also predicts the well-known phase jumps[17,28] of magnitude 2π which arise in a ring laser when noise momentarily overcomes the phase locking caused by backscattering.[16-18,21,24,28-32]

In light of this summary, in which a wide variety of lasers described by deterministic models exhibits phase jumps and intensity oscillations, it seems natural to ask if such behavior in the stochastic model arises from dynamics intrinsic to the deterministic portion of the Langevin equations, or whether the stochastic noise terms are its fundamental source. This paper addresses this question by removing the noise terms from the Langevin equations, solving the resulting deterministic equations, examining their behavior, and comparing this behavior with numerical simulations of the original Langevin equations and with experimental data. It will be shown that the solution to the deterministic equations is unique inside a certain domain in which intensity oscillations may exist, but no phase jumps. On the edge of this domain, however, the solution for the phase is no longer unique and is unstable. Once driven to this edge, the system may return via either of the two phase solutions. If it departs following the solution other than the one on which it arrived, a π or 2π phase jump occurs, depending upon conditions on the backscattering phases. Under these conditions, stochastic noise can serve to repeatedly drive the solution to this unstable boundary, and a series of random jumps occurs. When these conditions are relaxed,

the system deterministically evolves away from this boundary for all times, or it may pass through the boundary once and then never return. In this latter case, one transient *deterministic* π phase jump occurs. A series of deterministic jumps occurs if the system is continuously driven through the boundary. Other new results are mentioned, including an estimate for the average mode intensity in the presence of backscattering and a means to experimentally determine the operating point and backscattering coefficients for the laser. These results may be applied to lasers whose spontaneous emission noise is negligible, as for lasers operating far above threshold or lasers with large backscattering, or possibly FIR lasers.

II. GENERAL SOLUTION TO THE DETERMINISTIC THIRD-ORDER EQUATIONS

We start by presenting the dimensionless third-order Langevin equations just described, which assume zero detuning and include the effects of backscattering:[24–27]

$$\begin{aligned}\dot{\tilde{E}}_1&=(a_1-|\tilde{E}_1|^2-|\tilde{E}_2|^2)\tilde{E}_1+\tilde{R}_1\tilde{E}_2+\tilde{q}_1\ ,\\ \dot{\tilde{E}}_2&=(a_2-|\tilde{E}_1|^2-|\tilde{E}_2|^2)\tilde{E}_2+\tilde{R}_2\tilde{E}_1+\tilde{q}_2\ .\end{aligned}\tag{1}$$

Here $\tilde{E}_1$ and $\tilde{E}_2$ are the complex, dimensionless, slowly varying field variables for the two counterpropagating modes, a_1 and a_2 are their corresponding pump parameters, and $\tilde{R}_1$ and $\tilde{R}_2$ are the corresponding complex backscattering coefficients. Throughout this paper, we will set $a_1=a_2=a$ ($a>0$; see Appendix). For each mode, the complex noise terms $\tilde{q}_1$ and $\tilde{q}_2$ represent rapid spontaneous emission fluctuations and so we take them to be δ-correlated random variables of zero mean:

$$\langle q_i^*(t)q_j(t')\rangle=4\delta_{ij}\delta(t-t'),\quad i,j=1,2\ .\tag{2}$$

We now drop the noise terms and make the following substitutions:

$$\tilde{R}_j=R_je^{i\theta_j},\quad \tilde{E}_j=E_je^{i\phi_j},\quad j=1,2\ .\tag{3}$$

If we now separate the real and imaginary parts of the resulting equations and define $\alpha(t)$ and $\Delta\theta$ by

$$\theta_1+\theta_2=\pi+2\Delta\theta\ ,\tag{4}$$

$$\alpha(t)=\theta_1-\Delta\theta+\phi_2(t)-\phi_1(t)\ ,\tag{5}$$

then we arrive at the following three coupled real equations:

$$\dot{E}_1=(a-I_1-I_2)E_1+R_1E_2\cos(\alpha+\Delta\theta)\ ,\tag{6}$$

$$\dot{E}_2=(a-I_1-I_2)E_2-R_2E_1\cos(\alpha-\Delta\theta)\ ,\tag{7}$$

$$E_1E_2\dot{\alpha}=R_2I_1\sin(\alpha-\Delta\theta)-R_1I_2\sin(\alpha+\Delta\theta)\ ,\tag{8a}$$

or, for $E_1\neq0$ and $E_2\neq0$,

$$\dot{\alpha}=R_2\frac{E_1}{E_2}\sin(\alpha-\Delta\theta)-R_1\frac{E_2}{E_1}\sin(\alpha+\Delta\theta)\ ,\tag{8b}$$

in which we define the mode intensities by

$$I_j(t)=[E_j(t)]^2,\quad j=1,2\ .\tag{9}$$

We can show (see Appendix) that the solution (apart from the trivial unidirectional solution) to these equations is

$$I_j(t)=\frac{R_ja}{R_1+R_2}S_j(t)T(t),\quad j=1,2\tag{10}$$

with

$$\begin{aligned}S_1(t)&=1-A(t)\cos[\gamma(t)]\ ,\\ S_2(t)&=1+A(t)\cos[\gamma(t)]\ ,\\ \gamma(t)&=\omega_st+\beta\ ,\\ A(t)&=\operatorname{sech}(\kappa t+D)\ ,\\ \kappa&=-2\sqrt{R_1R_2}\sin(\Delta\theta)\ ,\\ \omega_s&=2\sqrt{R_1R_2}\cos(\Delta\theta)\ ,\end{aligned}\tag{11}$$

$$T(t)=\left[H(t)+CA(t)e^{-2at}+\left[\frac{R_2-R_1}{R_2+R_1}\right]\left[\frac{A(t)}{1+\omega_s^2/4a^2}\right]\left[\cos[\gamma(t)]+\frac{\omega_s}{2a}\sin[\gamma(t)]\right]\right]^{-1}\ ,\tag{12}$$

$$H(t)=\begin{cases}\left[\dfrac{4a^2}{4a^2-\kappa^2}\right]\left[1-\dfrac{\kappa}{2a}\tanh(\kappa t+D)\right], & |\kappa|\neq2a\\ 1+A(t)(at\,e^{-2at\mp D}-\frac{1}{4}e^{2at\pm D}), & \kappa=\pm2a\ .\end{cases}\tag{13}$$

$\alpha(t)$ is determined on the interval $-\pi$ to π by

$$\cos[\alpha(t)]=\frac{A(t)\sin[\gamma(t)]}{\sqrt{S_1(t)S_2(t)}}\ ,\tag{14}$$

together with

$$\sin[\alpha(t)]=\frac{\tanh(\kappa t+D)}{\sqrt{S_1(t)S_2(t)}}\ ,\tag{15}$$

for $A(t)<1$ or $A(t)=1$ with $\gamma\neq n\pi$. The peculiar case $A(t)=1$ with $\gamma=n\pi$ will be discussed later. The constants C and D and the angle β ($-\pi<\beta\leq\pi$) are determined from the initial conditions $I_1(0)=I_{10}$, $I_2(0)=I_{20}$, and $\alpha(0)=\alpha_0$ by the following relations:

$$D=\pm\operatorname{sech}^{-1}\left[1-\frac{4R_1R_2I_{10}I_{20}\sin^2(\alpha_0)}{(R_2I_{10}+R_1I_{20})^2}\right]^{1/2}\qquad\text{for }\sin(\alpha_0)\begin{cases}>0\\<0\end{cases},\tag{16}$$

$$\sin(\beta)=2\cos(\alpha_0)\cosh(D)\frac{\sqrt{R_1R_2I_{10}I_{20}}}{(R_2I_{10}+R_1I_{20})}\ ,$$
$$\cos(\beta)=-\cosh(D)\frac{(R_2I_{10}-R_1I_{20})}{(R_2I_{10}+R_1I_{20})}\ , \tag{17}$$

$$C=\cosh(D)\left[C'+\frac{2R_1R_2a}{(R_1+R_2)(R_2I_{10}+R_1I_{20})}\right]+\frac{(R_1-R_2)\left[\cos(\beta)+\frac{\omega_s}{2a}\sin(\beta)\right]}{(R_1+R_2)\left[1+\frac{\omega_s^2}{4a^2}\right]}\ , \tag{18}$$

$$C'=\begin{cases}-1+\dfrac{\mathrm{sech}(D)e^{\pm D}}{4}, & \kappa=\pm 2a\\ \dfrac{-4a^2\left[1-\dfrac{\kappa}{2a}\tanh(D)\right]}{(4a^2-\kappa^2)}, & |\kappa|\neq 2a\ .\end{cases}$$

For $\kappa\neq 0$, the time-dependent amplitude $A(t)$ decays to 0, so that $I_{1,2}$ and α undergo damped oscillations to steady-state values. We will return to this general case later.

III. SOLUTION FOR THE π PHASE-JUMP CONDITION

A. Form of the deterministic solution

For $R_1, R_2\neq 0$, κ equals zero provided $\Delta\theta=n\pi$. This condition on the backscattering phases will be referred to as the π-jump condition. In this case, $A(t)$ is now a constant which we call A. The solution for the intensities given by Eqs. (10) factors into a steady-state oscillation $S_{1,2}(t)$, an amplitude prefactor, and a factor $T(t)$ which is only a transient decay term if $R_1=R_2$. For $R_1\neq R_2$, this term also introduces a periodic modulation which distorts the shape of the intensity oscillations, and which causes the sum of the two intensities to oscillate.

The anticorrelated intensity oscillations are well known.[4,8,16,17,20,24–27,33–36] Earlier stability analyses[20] of the Langevin equations approximated the intensities by power series in the laser gain, which to first order demonstrated that oscillations occur in the intensities and their correlation functions with frequency equal to $2R_1$ for the special case $R_1=R_2$. This effect was verified experimentally for the cw dye ring laser.[36] Data and numerical solutions of Eqs. (1) were presented[26] to support a conjecture that Eqs. (11) gives the correct form for ω_s for the case $\Delta\theta=0$. Recently, a steady-state probability density has been derived[27] from the Langevin equations for the cases (i) $a_1\neq a_2$ with $\tilde{R}_1=\tilde{R}_2^*$ and (ii) $a_1=a_2$ with $R_1=R_2$. This solution relies upon a transformation whose effective eigenvalue has real and imaginary parts equal to half our ω_s and κ. It is significant that this transformation is valid even if $R_1\neq R_2$, although the resulting probability density is not. All these results are consistent with our equations. Comparisons will not be drawn here with experimental and theoretical work concerning oscillations induced by backscattering in solid state and semiconductor lasers[3,8,10,37] as the equations of motion for these lasers are somewhat different.

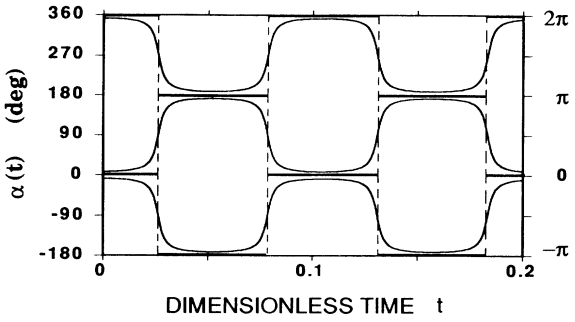

FIG. 1. The relative phase $\alpha(t)$ vs dimensionless time computed from Eqs. (10)–(18) for $a=10$, $R_1=R_2=30$, $A=0.99$ (curves), and $A=1$ (horizontal lines). The initial conditions are $I_{10}=I_{20}=1$ and $\alpha_0=-8.1°$, 8.1°, and 351.9°. The vertical dotted lines indicate the jump transitions between the unstable $A=1$ boundary lines. The adjacent phase trajectories are unique for $A<1$.

The shape of the solution for the relative phase $\alpha(t)$ is independent of R_1 and R_2, which only affect the oscillation magnitude A. For $\Delta\theta=0$, Eqs. (6) and (7) are even in α; for every solution of these equations with initial conditions I_{10}, I_{20}, and $n\pi-\alpha_0$ (for $-\pi\leq\alpha_0\leq\pi$), there is another solution corresponding to the initial conditions I_{10}, I_{20}, and $n\pi+\alpha_0$ whose intensities are the same as the first solution, but whose phase is a reflection of the first about the line $\alpha=n\pi$, as illustrated in Fig. 1. We consider α to be a cumulative phase difference which is not restricted to $(-\pi,\pi)$ so that solutions for the initial conditions α_0 and $2n\pi+\alpha_0$ are distinct curves. Figure 1 demonstrates that these solutions are distinct for $A<1$, but overlap for $A=1$. In Fig. 2, we plot the intensities

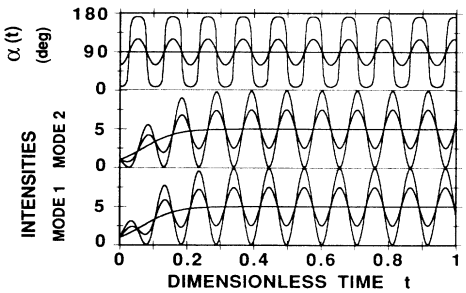

FIG. 2. Plots of the relative phase $\alpha(t)$ and the dimensionless intensities vs dimensionless time as computed from Eqs. (10)–(18) for $a=10$, $R_1=R_2=30$, and initial conditions $I_{10}=I_{20}=1$ and $\alpha_0=8.1°$, 60°, and 90° [yielding $A=0.99$ (large oscillations), 0.5 (small oscillations), and 0 (no oscillations), respectively].

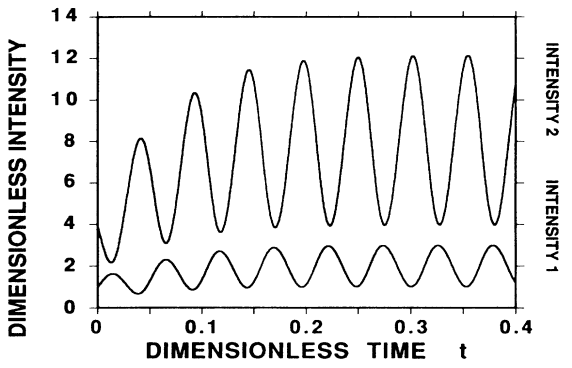

FIG. 3. Plots of dimensionless intensity vs dimensionless time as in Fig. 2 with $R_1=30$, $R_2=120$, $I_{10}=1$, $I_{20}=4$, and $\alpha_0=60°$ ($A=0.5$). Note that the oscillation period has decreased due to the larger R_1R_2 product.

and the phase $\alpha(t)$ as determined by Eqs. (10)–(18) for different values of A but with $R_1=R_2$. In Fig. 3, we plot the same quantities with constant A but with $R_1\neq R_2$ to illustrate the effect of changing R_1 and R_2 upon the period and amplitude of the oscillations.

B. Unstable behavior of the solution at $A=1$

Uniqueness of the solution for $A<1$ is insured by a generalization of Picard's Theorem to systems of more than one variable.[38] When $A=1$, uniqueness can fail for two reasons: (i) for $\gamma=\omega_s t+\beta=n\pi$, E_1 or E_2 becomes zero; (ii) for $\gamma\neq n\pi$, adjacent solutions overlap as previously described. We first treat the case for constant A, and return to the general case later.

To correctly describe the behavior at $A=1$, we must return to Eqs. (6), (7), and (8a). The solutions for $\sin(\alpha)$ and $\cos(\alpha)$ contain irremovable discontinuities at $\gamma=n\pi$ and are

$$\sin[\alpha(t)]=\begin{cases}0, & \gamma(t)\neq n\pi\\ \pm 1, & \gamma(t)=n\pi\end{cases}$$
$$\cos[\alpha(t)]=\begin{cases}\dfrac{\sin[\gamma(t)]}{|\sin[\gamma(t)]|}, & \gamma(t)\neq n\pi\\ 0, & \gamma(t)=n\pi\ .\end{cases} \tag{19}$$

This form for α implies that $\dot{\alpha}$ diverges whenever $\gamma=n\pi$. The discontinuities are rooted in the physical fact that the phase of the field is not defined when the field has zero magnitude. The result is that the phase does not evolve continuously, and undergoes jumps whenever $\gamma=n\pi$. This is illustrated in Fig. 1, in which the solid horizontal lines are the trajectories given by Eqs. (19) while the dotted lines indicate the jumps. Adjacent solutions for α converge to the same horizontal line, so the $A=1$ solution is not unique and the trajectory can jump either up or down to the next horizontal line. It is now apparent how π phase jumps occur: for $A<1$, the system approaches so close to the $\alpha=n\pi$ boundary that noise (spontaneous emission or other) drives it to the boundary. It may leave the boundary along the same trajectory with which it entered, or cross the boundary and leave via a solution which oscillates about a mean value of α which is shifted from the original one by π.

Any $A=1$ trajectory is orbitally stable[39] during times for which neighboring trajectories are converging towards it. Otherwise, it is unstable. It is apparent from Fig. 1 that the $A=1$ trajectories are most unstable as they approach the next time at which $\gamma=n\pi$. Therefore we expect most of the phase jumps to occur near this point, which is also the time when one of the intensities is zero. Just after this point, trajectories begin to converge toward the next horizontal line, so that there is a region of orbital stability until the system passes through a point of neutral stability at $\gamma=(n+\frac{1}{2})\pi$.

These arguments can be justified by utilizing linear stability analysis,[39] which determines the rate at which small fluctuations in the trajectories grow or contract in time. Rewrite Eqs. (6), (7), and (8b) in the vector form

$$\dot{\mathbf{u}}=\mathbf{F}(t)\ , \tag{20}$$

where $\mathbf{u}=(E_1,E_2,\alpha)$. Let $\mathbf{u}_0$ be a solution to Eq. (20) and let $\boldsymbol{\varepsilon}$ be a small perturbation of $\mathbf{u}_0$. Let us substitute into Eq. (20) the perturbed solution

$$\mathbf{u}=\mathbf{u}_0+\boldsymbol{\varepsilon}\ . \tag{21}$$

Retaining only terms linear in $\boldsymbol{\varepsilon}$, we arrive at

$$\dot{\varepsilon}_j=\sum_{k=1}^{3}\left|\frac{\partial F_j}{\partial u_k}\right|_{\mathbf{u}=\mathbf{u}_0}\varepsilon_k,\quad j=1,2,3\ . \tag{22}$$

These equations are quite complicated, as $\mathbf{F}$ is time dependent. However, for the case $A=1$ with $\gamma\neq n\pi$, the equations for $\dot{\varepsilon}_1$ and $\dot{\varepsilon}_2$ decouple from the equation for $\dot{\varepsilon}_3$. The result is that the time rate of fractional change in ε_3, defined as $\lambda(t)$, is given by

$$\lambda(t)=\dot{\varepsilon}_3/\varepsilon_3=-\omega_s\cot[\gamma(t)]\ . \tag{23}$$

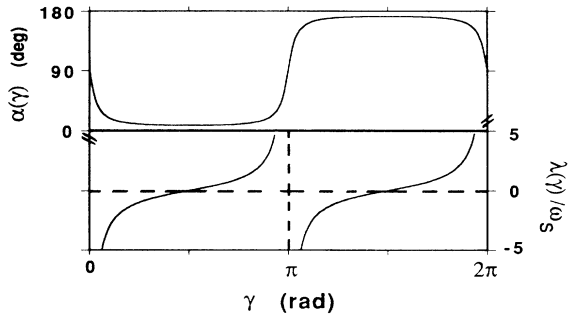

FIG. 4. Plot of the relative phase $\alpha(\gamma)$ for $A=0.99$ with the corresponding plot of $\lambda(\gamma)/\omega_s$, the normalized fractional rate of change of ε_3, together vs γ from Eq. (23). The $A=1$ solution is stable, marginally stable, or unstable for $\lambda(\gamma)$ less than, equal to, or greater than zero, respectively.

The $A=1$ solution is stable, marginally stable, or unstable when $\lambda(t)$ is less than, equal to, or greater than zero, respectively. In Fig. 4 we plot $\lambda(\gamma)/\omega_s$ and $\alpha(\gamma)$ together versus γ. The stability behavior is exactly as expected.

C. Correspondence with numerical solutions of the Langevin equations

We now compare these results with numerical solutions of Eq. (1) obtained by Monte Carlo simulations.[4,40] Figure 5 shows the time evolution of the relative phase $\alpha(t)$ and the intensity $I_1(t)$ during the course of several π jumps for $\Delta\theta=0$. Horizontal dotted lines indicate the $A=1$ boundary lines. The amplitude A of the phase oscillations is seen to increase near a transition. A trajectory may reach the boundary and return along the same trajectory (A), it may hover along the boundary and slowly cross to a π-shifted trajectory (B), or a rapid jump may occur (C). Due to the stability features of the $A=1$ trajectory discussed previously, large fluctuations away from the boundary occur only as the system approaches times which satisfy $\gamma=n\pi$, such as at (C). Otherwise, small fluctuations may drive the system back and forth across the boundary without a resultant large excursion away from it (A). Hence a distribution of time intervals between jumps will show peaks when either intensity is zero, which occur at times equal to multiples of π/ω_s. Although phase jumps may occur at other times, they are hard to identify, as their resultant excursions are very small. These conclusions may be substantiated by numerically computing a distribution of times T_J between jumps by defining a jump to occur whenever $\alpha(t)$ passes

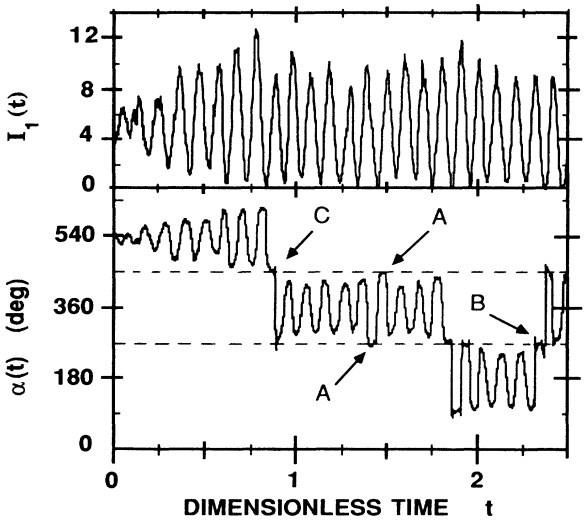

FIG. 5. Time evolution of the relative phase $\alpha(t)$ and the intensity $I_1(t)$ from numerical integration of Eqs. (1), with dimensionless iteration step size equal to 0.000 01, $a=10$, $R_1=R_2=30$, $\Delta\theta=0$. The oscillation amplitude A grows near a phase jump, but may equal 1 without a jump occurring, such as at (A).

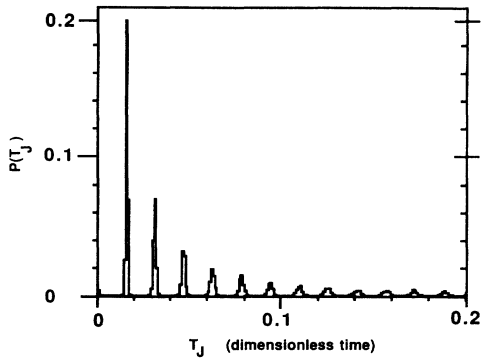

FIG. 6. The probability distribution $P(T_J)$ of the time intervals T_J between phase jumps, for $a=15$, $R_1=R_2=100$, and $\Delta\theta=0$, found through numerical integration of Eqs. (1), with iteration step size = 0.000 01. The distribution represents an ensemble average over five elements, each contributing 1000 intervals.

through a hysteresis band centered on the $A=1$ boundaries. Figure 6 shows a distribution of the probability $P(T_J)$ of a jump occuring at time T_J versus T_J. Due to large (90°) phase fluctuations which occasionally arise just before or after a jump, it is necessary to set the hysteresis bandwidth equal to 180°. The form of the distribution is as expected. The dimensionless time between peaks, 0.0157, corresponds to half the period of the intensity oscillations. The small peak at $T_J=0$ indicates that jumps of $n\pi$ ($n=\pm2,\pm3,\ldots$) are possible, but very unlikely for these initial conditions.

Previously[4] it was shown that phase jumps occur when $\tilde{R}_1+\tilde{R}_2^*=0$. Although this is sufficient, the foregoing analysis shows that equality of R_1 and R_2 is not necessary. Numerical simulations corroborate this. The mean time between phase jumps $\langle T_J\rangle$ is dependent upon a, R_1, R_2, and $\Delta\theta$. Figure 7 illustrates the dependence of $\langle T_J\rangle$ upon the pump parameter a and R_1 for $R_1=R_2$ and $\Delta\theta=0$. Phase jumps occur more frequently when the

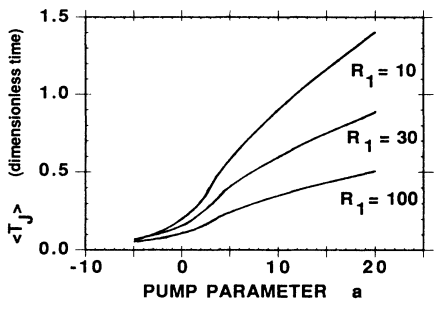

FIG. 7. Dependence of the mean time $\langle T_J\rangle$ between phase jumps upon pump parameter a and the backscattering coefficient $R_1=R_2$. The dimensionless iteration step size used in the numerical integration of Eqs. (1) is 0.000 01, and $\Delta\theta=0$. Due to the uncertainty in the ensemble average, the position of these curves is uncertain to 10%.

system is driven closer to threshold (by decreasing a or increasing R_1 or R_2) as the intensities have a greater chance of becoming zero.

IV. PHASE JUMPS IN THE GENERAL SOLUTION

A. Noise driven jumps

1. π jumps

a. Behavior of the deterministic solution. In the general case for which $\Delta\theta \neq n\pi$, phase jumps may still occur. In order to demonstrate that the magnitude of these jumps is still π, consider the limiting forms of Eqs. (14) and (15) as $\gamma \rightarrow n\pi$ and $\kappa t + D \rightarrow 0$ simultaneously:

$$\sin(\alpha) = \frac{\pm\kappa}{(\kappa^2+\omega_s^2)^{1/2}} , \qquad \cos(\alpha) = \frac{\pm\omega_s}{(\kappa^2+\omega_s^2)^{1/2}} . \tag{24}$$

The sign depends upon the direction from which we approach the limit. Hence, the general solution contains an irremovable discontinuity in α as in the $A=1$ case, and its uniqueness is insured except for $A(t)=1$. Although the value of α before and after the jump is different from the $A=1$ case, the magnitude of the jump is still π, as both $\sin(\alpha)$ and $\cos(\alpha)$ change sign. If $\gamma \not\rightarrow n\pi$ as $\kappa t + D \rightarrow 0$, the phase undergoes a continuous transition of magnitude π rather than a discontinuous jump, and neither intensity reaches 0.

b. Comparison with numerical integration of the Langevin equations. The preceding section demonstrates that the deterministic instability which allows π phase jumps to occur is still present for $\Delta\theta \neq n\pi$. We now discuss the effect of nonzero $|\kappa|$ upon the rate at which spontaneous emission noise drives the system across its unstable boundary. Equations (10)–(18) show that the intensity and phase oscillations decay to zero at a rate equal to $|\kappa|$, which in turn depends upon $\Delta\theta$, R_1, and R_2. Figure 8 shows the effect of this decay upon $\langle T_J \rangle$ as a function of $\Delta\theta$. Hence, random π phase jumps can occur even when the π-jump condition does not hold, but their frequency decreases with increasing $|\kappa|$. Therefore, in an experiment in which $\Delta\theta$ cannot be held precisely at zero, increasing $R_{1,2}$ may not decrease $\langle T_J \rangle$ but rather increase it by damping out $A(t)$. The effect of fluctuations in $\Delta\theta$ upon the distribution $P(T_J)$ is to increase $\langle T_J \rangle$ and to broaden the individual peaks, as their separation depends upon $\Delta\theta$. If the fluctuations are large enough, $P(T_J)$ may be continuously distributed.

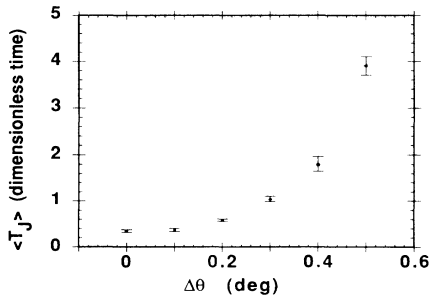

FIG. 8. Dependence of the mean time between phase jumps upon $\Delta\theta$. Numerical integration of Eqs. (1) utilized $R_1 = R_2 = 100$, $a = 10$, and a dimensionless iteration step size equal to 0.000 01. Each point is an ensemble average over five realizations, and its error bar represents the standard deviation of the five means. Each realization counts the time intervals between 1000 consecutive jumps.

2. 2π jumps

a. Behavior of the deterministic solution. When a ring laser operates below or near threshold and it is strongly influenced by stochastic noise, its phase may exhibit 2π phase jumps which are associated with the momentary unlocking of its modes.[17,28] Although our solution is not valid under these conditions, we may still examine it for an intrinsic instability which may contribute to this effect. Consider first the extreme case in which $\Delta\theta = \pm\pi/2$ (with $\beta \neq n\pi$). Here, $\omega_s = 0$ and $|\kappa|$ is at its maximum, so $\alpha(t)$ rapidly decays without oscillation towards its asymptotic (steady-state) value of $2n\pi \mp \pi/2$ for $\Delta\theta = \pm\pi/2$ (cf. Eqs. 10–15). Hence, for fixed $\Delta\theta \neq 0$, the steady-state values of α are separated by 2π. The instability at $t = -\kappa/D$ is still present, but if the phase is driven to this point from an initial steady-state value and undergoes an $n\pi$ jump, afterwards it must evolve towards another steady-state value shifted by $2n\pi$ relative to its initial one.

Consider the two curves for $\alpha(t)$ generated from the initial conditions $\alpha_{\pm}(t \rightarrow -\infty) = -\pi/2 \pm \delta$ with $\delta > 0$ but arbitrarily small. Initially close together, these trajectories evolve to values separated by 2π: $\alpha_{\pm}(t \rightarrow \infty) = -\pi/2 \pm \pi$. More generally, for the family of curves of $\alpha(t)$ generated from the set of initial conditions $\alpha(t \rightarrow -\infty) = 2n\pi - \pi/2$ (analogous to Fig. 1, but with $\Delta\theta = -\pi/2$), the horizontal lines $\alpha(t) = 2n\pi - \pi/2$ are unstable boundaries which separate regions whose asymptotic values of α differ by 2π. For $\Delta\theta = \pi/2$, the unstable boundaries are the lines $\alpha(t) = 2n\pi + \pi/2$.

For $\Delta\theta \neq \pm\pi/2$, oscillations in α can drive it across these boundaries, so the direction of the phase jump is determined by the behavior of $\cos\alpha$ when $t = -\kappa/D$. As $\cos\Delta\theta$ becomes large, crossings rapidly occur and the decay to the steady state slows, so the dynamics become those of π rather than 2π jumps.

b. Comparison with analytical results from the Fokker-Planck equation. The boundary lines discussed in the preceding section correspond exactly to the maxima of a sinusoidal potential in which a hypothetical particle (representing the phase) moves under the influence of random noise.[23,28] The positions of the minima of this potential are separated by 2π and are the steady-state phase values just discussed.

c. Comparison with numerical integration of the Langevin equations. Numerical solutions to (1) establish other correspondences with our analytical solution. They

confirm that the phase jump is associated with an intensity becoming zero, which occurs at our instability. However, studies[25] of the effects of backscattering on the intensity cross correlation show that the intensities are positively correlated close to threshold. Therefore, whereas π jumps are associated with anticorrelated intensities and a zero crossing of one field amplitude, 2π jumps are associated with correlated intensities and zero crossings of both field amplitudes. Although our solution does predict identical behavior for the two intensities when $\Delta\theta=\pm\pi/2$ with $R_1=R_2$ and $I_{10}=I_{20}$, it does not allow for both intensities to become zero simultaneously. A distribution of time intervals between 2π jumps similar to Fig. 6 reveals a continuous distribution with approximately exponential form, as expected for phase jumps driven by random noise rather than the periodic zero crossings of anticorrelated amplitudes. Numerical studies similar to those used in Fig. 7 show that these jumps become more frequent with decreasing a and R, consistent with threshold operation and a decreasing rate of decay to the steady state, $|\kappa|$. Finally, computations similar to those used in Fig. 8 show that jumps near threshold occur over a wide range of $\Delta\theta$. We will not discuss this in greater depth, as our solution has very limited validity in this region.

B. Transient deterministic jumps

In addition to these noise-driven jumps, the deterministic equations alone allow for a single transient π jump (or transition) to occur for arbitrary $\Delta\theta$. If the deterministic system is started such that $A(t)$ initially evolves towards its maximum (at $t=-\kappa/D$) rather than away from it, one of the following will happen there: (i) for $\gamma=n\pi$, one intensity will become zero and a discontinuous jump occurs, or (ii) for $\gamma\neq n\pi$, neither intensity becomes zero and a continuous transition occurs. Figure 9 shows plots of $I_1(t)$, $I_2(t)$, and $\alpha(t)$ given by Eqs. (10)–(18) for these cases. In Fig. 9(a), $\Delta\theta=-4°$ and $A(t)\cong 1$ at the jump. In Fig. 9(b), $\Delta\theta=-60°$ and $A(t)$ is never very close to 1. The other parameters are the same for each plot: $a=10$, $R_1=R_2=10$, $\alpha_0=270°$, $I_{10}=20$, and $I_{20}=10$. Figure 9 also illustrates the effect of changing $\Delta\theta$ upon the period of the oscillations and their decay time. In an experiment, it may be possible to generate a series of jumps by operating the system far from threshold, but continuously resetting the system to a state which will evolve through $A(t)=1$. These jumps can be distinguished from the stochastic ones as the phase oscillations rapidly damp out and the system phase will lock (compare Figs. 5 and 9).

C. Steady-state deterministic jumps

If $\sin(\Delta\theta)$ is driven through 0 so slowly that the transients may always be considered to have relaxed to zero, a deterministic phase jump still occurs at the zero crossing. This is distinct from the transient response just discussed, as it is exhibited in the steady-state phase behavior and only occurs when $\Delta\theta$ crosses $n\pi$. For $t\to\infty$ and $\Delta\theta\neq n\pi$, Eqs. (5), (10)–(18) yield

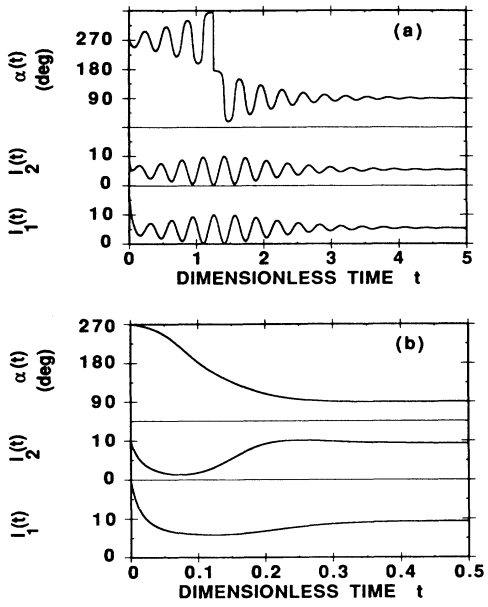

FIG. 9. Time evolution of the relative phase $\alpha(t)$ and the intensities from Eqs. (10)–(18). If the system is started so that it deterministically evolves through the maximum of the amplitude function $A(t)$ then either a single (a) discontinuous phase jump or (b) continuous transition occurs. The parameters used to generate the curves are identical except that $\Delta\theta=-4°$ for (a) and $\Delta\theta=-60°$ for (b).

$$I_j=\frac{R_j}{R_1+R_2}(a+\sqrt{R_1R_2}\,|\sin(\Delta\theta)|),\quad j=1,2$$
$$\phi=\phi_2-\phi_1=\Delta\theta-\theta_1\mp\frac{\pi}{2}\ \text{for}\ \sin(\Delta\theta)\gtrless 0\ . \tag{25}$$

For $\Delta\theta\to n\pi$, Eqs. (25) give the mean values for the oscillating intensities and phase. In Fig. 10 we plot $I_1(t\to\infty)$

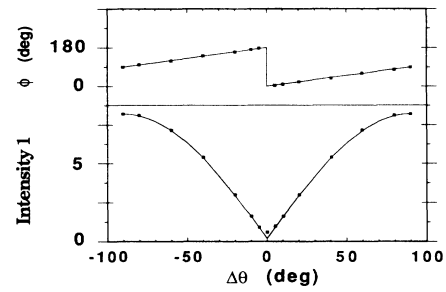

FIG. 10. Agreement between the dimensionless intensity I_1 and the relative phase ϕ computed from Eqs. (25) (solid curve) and the ensemble averages for the intensity and phase determined by numerical integration of Eq. (1) (solid points) as a function of $\Delta\theta$ for $R_1=20$, $R_2=80$, and $a=1$. Each solid point is an ensemble average over 10 realizations of Eqs. (1), integrated with dimensionless step size equal to 0.000 01. The standard deviations of the ensemble means are approximately 0.1 times the size of the solid point.

and $\phi(t\rightarrow\infty)$ versus $\Delta\theta$ for $a=1$, with $R_1\neq R_2$. ϕ linearly follows $\Delta\theta$ except at a jump. Independent of how slowly the zero of $\sin(\Delta\theta)$ is crossed, a π phase jump must be present in the steady-state response.

D. Modulated deterministic phase jumps

If $\Delta\theta$ is sinusoidally varied about 0 (for $D=0$) in such a way that the system never has time to fully relax, then α exhibits a combination of the two forms of phase jumps (or transitions) just discussed. Theoretical and experimental work concerning this behavior is presented elsewhere,[41] but for completeness, we summarize the results here.

(i) At slow modulation frequencies, the jumps occur when $\Delta\theta=n\pi$, and oscillations in the phase and the intensities die out between jumps.

(ii) As the modulation frequency approaches ω_s the transient response does not have time to decay before the next zero crossing, so phase and intensity oscillations persist. The periodic jumps no longer occur at $\Delta\theta=n\pi$, as the laser response lags behind the modulation.

(iii) The directions of the phase jumps in this case are very sensitive to initial conditions, and are in this sense chaotic.

(iv) For modulation frequencies on the order of ω_s (depending upon the amplitude of the modulation), the phase jumps abruptly cease, as $A(t)$ is damped away from 1. For still greater modulation frequencies, the laser phase and intensities exhibit increasingly smaller fluctuations about steady-state values.

The distinguishing characteristic of this case is that variations in both $\Delta\theta$ and time affect the laser.

V. APPLICATIONS

A. Estimates of the mode intensities

For $\kappa\neq 0$, the steady-state mode intensities of the laser are given by Eqs. (25) provided that spontaneous emission can be neglected. Previous work led to an expression for the sum of the average mode intensities[24] resulting from an analysis of Eqs. (1), which included the effects of noise, but which required $R_1=R_2$ and the pump parameter to be far above threshold. This expression is a special case of Eq. (25). Recently, this result has been generalized[27] for arbitrary a. To illustrate the failure of our intensity equations at low pump parameters, we superimpose upon the curves of Fig. 10 the corresponding ensemble averages computed from numerical solution of (1), which includes the effects of the noise terms. The agreement fails for small $\Delta\theta$, as the effects of the noise terms are no longer negligible. At $\Delta\theta$ equal to 0° and 5°, the disagreements are 10 and 1 times the standard error of the ensemble means, respectively. This disagreement at $\Delta\theta=0$ decreases with a and is under 5% for $a=10$. The agreement also improves with increased $|\kappa|$, as the effect of the backscattering is to increase the effective pump parameter.[24]

B. Estimate of the operating point of the laser

Equations (25) may be used in an experiment to determine R_1, R_2, a, and $\Delta\theta$ for a ring laser. This is useful, as voltages or currents usually control these parameters, but the actual parameter values may not be known. Even if backscattering is facilitated by means of calibrated retroreflectors external to the laser cavity,[4,25,42] the coupling of the retroreflected beams into the cavity modes cannot be precisely known, as it depends upon beam geometry. The following is a method which allows for the determination of the parameters through a series of intensity measurements, and avoids having to estimate mirror reflectivities, quantum efficiencies, or retroreflected beam coupling. Inside the cavity, the steady-state intensities are given by Eqs. (25). Outside the cavity, a detector measures

$$I_j^M=\eta_j I_j,\quad j=1,2 \tag{26}$$

where η_j accounts for the optical losses from inside the cavity to the detector, the detector's efficiency, and subsequent amplification and measurement of its output. Plots of I_j^M versus $|\sin(\Delta\theta)|$ will be straight lines given by

$$I_j^M=m_j|\sin(\Delta\theta)|+b_j \tag{27}$$

with

$$b_j=\frac{\eta_j R_j a}{R_1+R_2},\ m_j=\frac{\eta_j R_j\sqrt{R_1R_2}}{R_1+R_2},\quad j=1,2\ .$$

Hence, we can obtain the ratio

$$\frac{m_j}{b_j}=\frac{\sqrt{R_1R_2}}{a}.\quad j=1,2 \tag{28}$$

For $\Delta\theta=n\pi$, the intensities undergo steady-state oscillation with unscaled frequency Ω_s, which may be computed from a time record of the intensities. To convert to the dimensionless frequency ω_s, we use the relationship[24] between unscaled time t and dimensionless time t':

$$t'=\sqrt{SB}\,t \tag{29}$$

in which S is the additive noise strength and B is the saturation coefficient. This will determine both a and the product R_1R_2. The scale factor can be experimentally determined beforehand through a series of equal time and time-dependent correlation measurements.[25,42]

Suppose R_2 is varied and several sets of data are recorded. For each set, R_2 is increased by an unknown factor c, so that $R_2(c)=cR_2$, and m_j and b_j become $m_j(c)$ and $b_j(c)$. The factor c can be determined from Eqs. (27) by

$$c=\frac{R_2(c)}{R_2}=\frac{b_1b_2(c)}{b_2b_1(c)}\ . \tag{30}$$

In order to determine c, we have assumed Eqs. (27) hold and have utilized b_j values for both modes. Therefore, the data sets for each mode are no longer independent in any subsequent calculation involving c, and so we must use only one set. Suppose we choose only the data set for

mode 1 and plot $1/b_1(c)$ versus c. This relation is

$$\frac{1}{b_1}=\frac{1}{\eta_1 a}+\frac{R_2 c}{R_1\eta_1 a} . \tag{31}$$

From a series of experimental measurements we can determine the slope and vertical intercept for Eq. (31), whose ratio for mode 1, W_1, is

$$W_1=R_2/R_1 . \tag{32}$$

Then, from having already determined ω_s, we have

$$R_2=\omega_s\sqrt{W_1}/2 . \tag{33}$$

Finally, we may calculate the ratio

$$\frac{\eta_1}{\eta_2}=\frac{b_1 W_1}{b_2} . \tag{34}$$

Thus we have determined R_1, η_1, η_2, a, and the set of R_2 values utilized in an experiment.

VI. COMPARISON WITH EXPERIMENTAL RESULTS

We now describe an experiment to verify several of these results. Figure 11 illustrates the apparatus, which is similar to that reported previously.[4,25,26,42] The He-Ne bidirectional ring cavity (made by Honeywell) has three mirrors, two of which are output couplers and the other is used to piezoelectrically tune the cavity to line center. Portions of the exiting light waves are retroreflected into the cavity with controlled amplitude and phase. A single retroreflector consists of a variable liquid-crystal polarization rotator positioned between two linear polarizers. The second polarizer has a mirror coating on its exit face. Retroreflector two is used to vary the phase by mounting its second polarizer on a piezoelectric driver. A portion of the remainder of the laser output is recorded by intensity monitors [photomultiplier tubes (PMT) 1 and 2] while the other part generates an interference pattern at a beam splitter. The fringes are enlargened by lenses, and a fraction of each fringe passing through a pinhole is recorded (PMT 3 and 4). By adjustment of the pinholes normal to the beam directions, PMT 3 and 4 can be made to measure light intensities at different fringe positions. Each PMT is an RCA 1P21 photomultiplier tube whose output current is integrated, amplified, and converted to a voltage signal. These signals are simultaneously recorded by four DSP Technology analog- to- digital converters which have 12-bit precision and a 2-MHz bandwidth. Time records of the intensities are read from these units into a PDP-11/73 computer via CAMAC for subsequent analysis.

The relative phase $\phi(t)$ is reconstructed from the four recorded intensities in the following manner. Let $I_j^M(t)$ be the measured intensity at PMT j ($j=1,\ldots,4$). We can show that

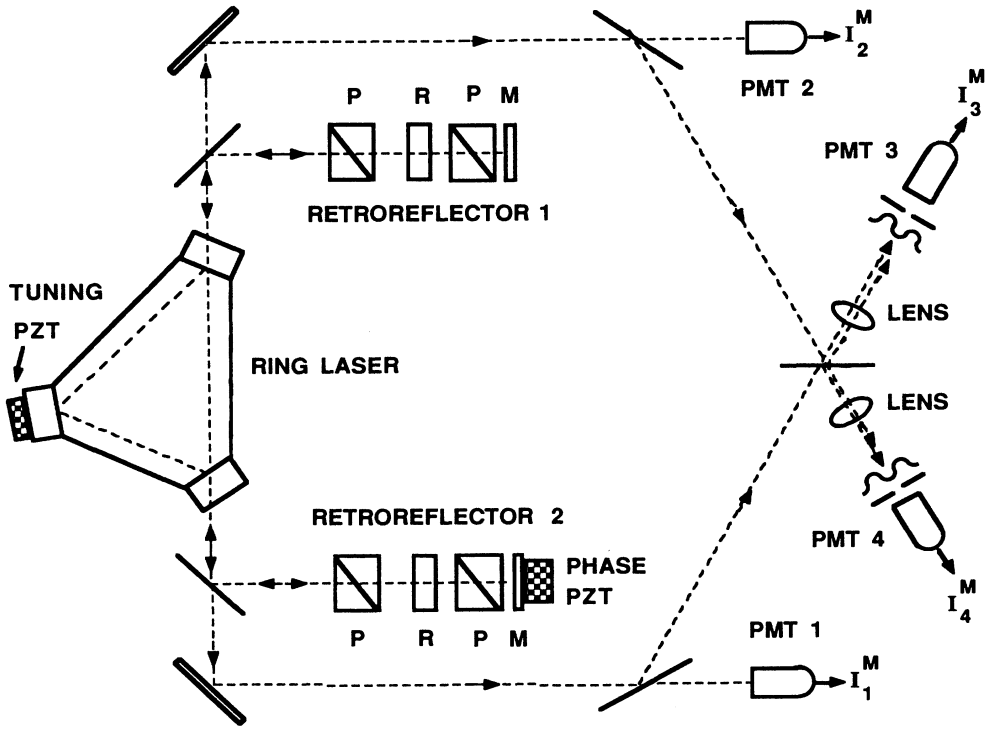

FIG. 11. The experimental apparatus. Each retroreflector consists of two polarizers (P), an electronically variable liquid-crystal rotator (R), and an end mirror (M). The laser cavity and the mirror of retroreflector 2 are adjusted by piezoelectric tuners (PZT).

$$
\begin{aligned}
I_3^M(t) &= \eta_{31} I_1^M(t) + \eta_{32} I_2^M(t) \\
&\quad + 2(\eta_{31}\eta_{32} I_1^M(t) I_2^M(t))^{1/2} \cos[\phi(t)] , \\
I_4^M(t) &= \eta_{41} I_1^M(t) + \eta_{42} I_2^M(t) \\
&\quad + 2(\eta_{41}\eta_{42} I_1^M(t) I_2^M(t))^{1/2} \cos[\phi(t) + \Delta\phi] ,
\end{aligned} \tag{35}
$$

where the η_{ij} account for beam splitter reflectivities, other optical losses, and detector signal processing. The constants η_{ij} are determined by alternately blocking light beams 1 and 2 while recording the intensities. Inverting each equation separately determines the argument of each cosine up to an overall sign. For fixed nonzero $\Delta\phi$, comparison of these four arguments yields only one pair which agree upon a value for $\phi(t)$. Alternatively, $\cos[\phi(t)+\Delta\phi]$ may be rewritten in terms of $\sin[\phi(t)]$ and $\cos[\phi(t)]$; then $\sin[\phi(t)]$ is determined and $\phi(t)$ can be reconstructed over $(-\infty, \infty)$. In practice, $\phi(0)$ and $\Delta\phi$ are determined at $t=0$ [when $\phi(t)$ is slowly varying] by choosing the positive arguments in Eq. (35). $\Delta\phi$ is varied by translating the pinhole for detector 4 as described.

In order to obtain measurements of the intensities and ϕ versus $\Delta\theta$ a slow (20-mHz) sawtooth voltage is applied to the piezoelectric driver in retroreflector 2. The four intensities are measured, and ϕ is reconstructed. Figure 12 shows the two measured mode intensities and ϕ as functions of $\Delta\theta$. The sampling rate was 10 samples/sec and the total sampling time was approximately 100 seconds. The horizontal axis is calibrated from the positions of the minima of the intensities, which are separated by 180°. The sharp features at the minima are due to incomplete sampling of the oscillations which occur there. For these data, ω_s (at $\Delta\theta=0$) will be shown to be 20 krad/sec or 1.2×10^6 deg/sec, which is much greater than the 4°/sec ramp rate for $\Delta\theta$. Therefore, the steady-state results are expected to hold except within approximately 0.2° of $\Delta\theta = n\pi$. The behavior of both the phase and intensities is exactly as expected from the steady-state equations [cf. Fig. 10 and Eq. (25)]. To examine the behavior at a jump, we record the intensities at a rate of 10 ksamples/sec near $\Delta\theta=0$ while ramping $\Delta\theta$ at 2°/sec. The results of the measurement are presented in Fig. 13. The horizontal scale is calibrated by performing an additional scan to obtain the separation between intensity minima, but the absolute position of $\Delta\theta=0$ is chosen to coincide with the phase jump shown. Oscillations in the intensities and in ϕ die out completely by $\Delta\theta=0.2°$. Since oscillations persist for $\Delta\theta\neq0$, the steady state is not attained, despite the fact that ω_s is 3×10^5 times greater than the rate of change of $\Delta\theta$. On this scale, the jump must be modeled as a driven jump (Sec. IV D) for which transients persist. We will not pursue this case here, but note that the intensity and phase oscillations are highly correlated and build up to full scale at a jump, as predicted.

In order to determine the operating point of the laser, a series of 11 scans similar to that of Fig. 12 was made. Following the procedure of Sec. V B, I_j^M is plotted versus $|\sin(\Delta\theta)|$. Only at small $\Delta\theta$ are all these curves linear, so the values of m_j are extracted for $\Delta\theta<20°$. Inconsistent results for m_j are obtained at larger $\Delta\theta$ values due to contributions from three mechanisms: (i) interferometer drift during the course of a scan, (ii) intrinsic backscattering internal to the triangular cavity, and (iii) periodic variations in R_2 due to slight displacements of the retroreflected beam as the retroreflector mirror is ramped. Extracting m_j near $\Delta\theta=0$ insures that the magnitudes R_1 and R_2 have not varied from their values at $\Delta\theta=0$, where the b_j are determined. $\tilde{R}_1$ and $\tilde{R}_2$ are actually effective backscattering coefficients, containing contributions from the intrinsic backscattering of the cavity. Numerical computations which include intrinsic backscattering have been performed, and they predict that (i) the mode intensities may peak at different $\Delta\theta$ values and (ii) using their heights to determine the m_j results in inconsistent values for a [if it is calculated ac-

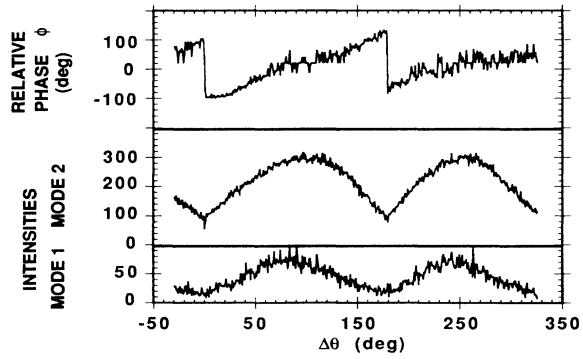

FIG. 12. Plot of the experimental intensities (arbitrary units) and relative phase vs $\Delta\theta$. A linear ramp voltage is applied to the mirror piezo of retroreflector 2 to vary $\Delta\theta$. All data shown were recorded on the same rising cycle of the ramp. The relative intensity scaling is that of the intracavity intensities, determined by dividing the measured intensities by the η_j values. Here, $a=160$, $R_1=190$, and $R_2=2193$.

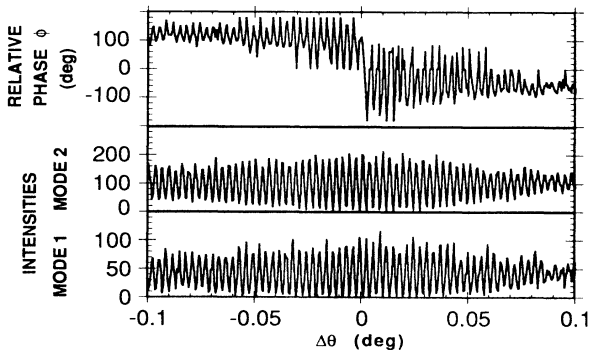

FIG. 13. Plot of the experimental intensities (arbitrary units) and relative phase vs $\Delta\theta$ in the region of a phase jump. The relative intensity scaling is identical to that of Fig. 12. The laser's operating parameters are the same as in Fig. 12, except that $R_2=510$. The oscillation frequency is 1.7 kHz.

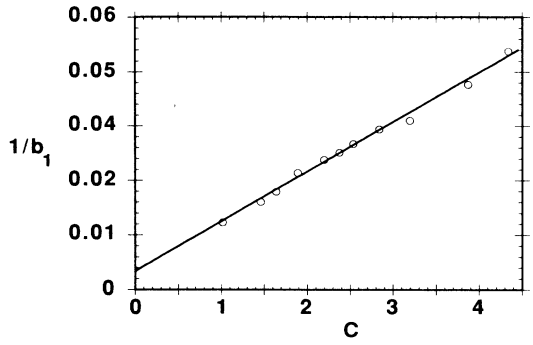

FIG. 14. Plot of $1/b_1$ vs c determined from the 11 sets of experimental data according to Eqs. (27) and (30), so to fit these data to Eq. (31). Superimposed upon the data is the best-fit line whose slope and intercept are 0.010 95 and 0.004 06, respectively.

cording to Eq. (28)]. These effects are observed in the data from several scans, but are not as apparent in scans with large external backscattering, as in Fig. 12. Although such calculations may be used in principle to determine the intrinsic backscattering characteristics, they will not be further discussed here.

From the data set displayed in Fig. 13, Ω_s is determined to be 11×10^3 rad/sec. Using Eq. (29) with the conversion factor reported earlier,[4] we find that $\omega_s=620$ rad/dimensionless time. From a data set similar to Fig. 12 but with operating parameters corresponding to those in Fig. 13, Eq. (28) yields $a=160$ for both modes. We take this set to correspond to $c=1$, and plot $1/b_1$ versus c in Fig. 14 to fit the 11 scans to Eq. (31). From a and the y intercept, we determine that $\eta_1=1.54$ and from ω_s and the slope we find $R_1=190$ and $R_2=510$ for $c=1$. Equation (34) yields $\eta_2=0.831$. By rescaling R, we can show[24] that a R_2 value of 510 corresponds to scattering 10 ppm of the amplitude of mode 1 into mode 2. Despite the large backscattering and pump levels used in these experiments, a simple calculation[14,42,43] shows that third-order theory is still a reasonable approximation.

VII. CONCLUSIONS

Although our model is limited due to its exclusion of additive noise terms, it compares well with the results of numerical solutions of the Langevin equations and with experiments, provided that the effective pump parameter (which includes backscattering) is large. Not only is steady-state behavior well described, but it gives much insight into time-dependent effects not accessible through the steady-state probability solution to the Fokker-Planck equation corresponding to Eq. (1), especially the phase-jump instability. This earlier work showed that the condition $\tilde{R}_1+\tilde{R}_2^*=0$ is sufficient for π jumps. This paper demonstrates that the equality of R_1 and R_2 is not required, nor need $\Delta\theta$ be zero for jumps to occur.

The following four cases of phase jumps may be identified: (i) random jumps driven by stochastic noise (a) of magnitude π for $\Delta\theta$ near $n\pi$ and the laser far above threshold, (b) of magnitude 2π for $\Delta\theta$ near $\pm\pi/2$ and the laser near or below threshold; (ii) a single deterministic transient π jump or transition for arbitrary $\Delta\theta$; (iii) a deterministic π jump in the steady state equations at $\Delta\theta=n\pi$; (iv) a series of π phase jumps or transitions driven by a deterministic source, which need not occur at $\Delta\theta=n\pi$, and which abruptly cease for driving frequencies on the order of the natural oscillation time of the system, depending upon the amplitude of the modulation.

For $\Delta\theta=n\pi$ or for $t=-\kappa/D$ with $\gamma=n\pi$, the π jumps must be discontinuous and one intensity must reach zero. Otherwise, continuous transitions occur; these require one intensity to reach its minimum, but it will not become exactly zero. Numerical work indicates that 2π jumps are associated with positively correlated intensities which are both near or equal to zero at a jump.

VIII. ACKNOWLEDGMENTS

The author thanks Dr. L. Mandel for his guiding advice, helpful criticism, and for the suggestion that driven phase jumps be investigated. The laser was donated by Honeywell. Much of the apparatus utilized with the laser originally was designed and constructed by Dr. W. R. Christian. Dr. E. C. Gage wrote the first versions of the digitizer programs. The author is indebted to Dr. E. C. Gage, Dr. W. R. Christian, Dr. N. B. Abraham, Dr. G. L. Lippi, and Dr. L. Hoffer for many beneficial conversations. The author thanks Dr. L. Pesquera and Dr. T. Ogawa for bringing their investigations to his attention. This work was supported in part by grants from the National Science Foundation and from the Office of Naval Research.

APPENDIX: METHOD OF SOLUTION

The purpose of this appendix is to outline the method of solution of the three nonlinear differential equations (6)–(8). That their solution exists in the factored form of Eq. (10) is due to the fact that Eqs. (6) and (7) share a common nonlinear term. If this is not true, i.e., for unequal pump parameters or unequal self- and cross-coupling coefficients, then the method discussed here fails. (In these cases, the solution is quite complicated and will be discussed elsewhere.)

The solution for $\Delta\theta=0$ with $R_1=R_2$ is obtained by first noticing from numerical work and experimental data that the steady-state solution is oscillatory, and that the modes are antiphase. This trial solution for S_1 and S_2 is substituted into an equation formed from the difference of multiples of Eqs. (6) and (7) contrived so that both $T(t)$ and the nonlinear term cancel. This generates an equation for $\cos(\alpha)$ and the equation for ω_s. It is then proven that this solution for $\cos(\alpha)$ satisfies Eqs. (8). Substitution back into Eq. (6) or Eq. (7) yields a nonlinear differential equation for $T(t)$ which can be solved by a series of substitutions. For unequal R_1 and R_2, the procedure is the same, but the calculations more complicated.

For $\Delta\theta\neq0$, the difference equation is solved with the assumption that A is a function of time. This yields a

nonlinear differential equation for $A(t)$, which can be solved by substitution, and which gives the equation for κ. This solution is then shown to satisfy Eqs. (8). The differential equation for $T(t)$ is solved by using a trial solution found by substituting $A(t)$ for all A's in the $\Delta\theta=0$ solution for $T(t)$, and including in $T(t)$ the arbitrary function $H(t)$ [see Eqs. (12)]. A nonlinear differential equation for $H(t)$ is then generated. It must be solved under the two separate cases indicated in Eqs. (13) by substitutions. In all cases, the remaining constants are easily determined from appropriate initial conditions.

[1]T. Ogawa and E. Hanamura, Opt. Commun. **61**, 49 (1987); Appl. Phys. B **43**, 139 (1987).

[2]L. M. Hoffer, G. L. Lippi, N. B. Abraham, and P. Mandel, Opt. Commun. **66**, 219 (1988).

[3]I. P. Efanova and E. G. Lariontsev, Zh. Eksp. Teor. Fiz. **55**, 1532 (1968) [Sov. Phys.—JETP **28**, 802 (1969)].

[4]W. R. Christian, T. H. Chyba, E. C. Gage, and L. Mandel, Opt. Commun. **66**, 238 (1988).

[5]C. O. Weiss, N. B. Abraham, and U. Hubner, Phys. Rev. Lett. **61**, 1587 (1988).

[6]N. B. Abraham and C. O. Weiss, Opt. Commun. **68**, 437 (1988).

[7]H. Zeghlache, P. Mandel, N. B. Abraham, L. M. Hoffer, G. L. Lippi, and T. Mello, Phys. Rev. A **37**, 470 (1988).

[8]B. L. Zhelnov, A. P. Kazantsev, and V. S. Smirnov, Zh. Eksp. Teor. Fiz. **50**, 1291 (1966) [Sov. Phys.—JETP **23**, 858 (1966)]; Y. L. Klimontovich, P. S. Landa, and E. G. Lariontsev, Zh. Eksp. Teor. Fiz. **52**, 1616 (1967) [Sov. Phys.—JETP **25**, 1076 (1967)]; G. V. Perevedentseva, P. A. Khandokhin, and Ya. I. Khanin, Kvant. Electron. (Moscow) **7**, 128 (1980) [Sov. J. Quantum. Electron. **10**, 71 (1980)].

[9]G. L. Lippi, J. R. Tredicce, N. B. Abraham, and F. T. Arrechi, Opt. Commun. **53**, 129 (1985); J. R. Tredicce, G. L. Lippi, F. T. Arecchi, and N. B. Abraham, Philos. Trans. R. Soc. London Ser. A **313**, 411 (1984).

[10]See, for example, E. L. Klochan, L. S. Kornienko, N. V. Kravtsov, E. G. Lariontsev, and A. N. Shelaev, Zh. Eksp. Teor. Fiz. **65**, 1344 (1973) [Sov. Phys.—JETP **38**, 669 (1974)]; M. V. Danileiko, A. L. Kravchuk, V. N. Nechiporenko, A. M. Tselinko, and L. P. Yatsenko, Kvant. Electron. (Moscow) **13**, 2147 (1986) [Sov. J. Quantum Electron. **16**, 1420 (1986)].

[11]C. O. Weiss and W. Klische, Opt. Commun. **51**, 47 (1984).

[12]H. Haken, Phys. Lett. **53A**, 77 (1975).

[13]C. O. Weiss and J. Brock, Phys. Rev. Lett. **57**, 2804 (1988).

[14]W. E. Lamb, Jr., Phys. Rev. **134A**, 1429 (1964); M. Sargent III, M. O. Scully, and W. E. Lamb, Jr., *Laser Physics* (Addison-Wesley, Reading, MA, 1974).

[15]H. Haken, in *Laser Theory,* Vol. XXV 2C of *Encyclopedia of Physics,* edited by S. Flugge (Springer-Verlag, Berlin, 1970).

[16]F. Aronowitz and R. J. Collins, Appl. Phys. Lett. **9**, 55 (1966).

[17]F. Aronowitz, in *Laser Applications,* edited by M. Ross (Academic, New York, 1971).

[18]L. N. Menegozzi and W. E. Lamb, Jr., Phys. Rev. A **8**, 2103 (1973).

[19]J. B. Hambenne and M. Sargent III, IEEE J. Quantum Electron. QE-**11**, 90 (1975).

[20]D. Kuhlke and G. Jetschke, Physica **106C**, 287 (1981); D. Kuhlke and R. Horak, *ibid.* **111C**, 111 (1981).

[21]J. D. Cresser, W. H. Louisell, P. Meystre, W. Schleich, M. O. Scully, Phys. Rev. A **25**, 2214 (1982).

[22]S. Singh, Phys. Rev. A **23**, 837 (1981).

[23]S. Singh, Phys. Rep. **108**, 217 (1984).

[24]W. R. Christian and L. Mandel, Phys. Rev. A **34**, 3932 (1986); Phys. Rev. A. **36**, 1510 (1987).

[25]W. R. Christian and L. Mandel, J. Opt. Soc. Am. B **5**, 1406 (1988).

[26]T. H. Chyba and L. Mandel, in *Optical Society of America Annual Meeting, 1988 Technical Digest Series* (Optical Society of America, Washington D.C., 1988), Vol. 11, p. 135.

[27]L. Pesquera, R. Blanco, and M. A. Rodriguez, in *Dynamics of Nonlinear Optical Systems,* edited by F. J. Bermejo and L. Pesquera (World Scientific, Philadelphia, 1989); Phys. Rev. A **39**, 5777 (1989); and unpublished.

[28]R. L. Stratonovich, *Topics in the Theory of Random Noise* (Gordon and Breach, New York, 1967).

[29]P. H. Lee and J. G. Atwood, IEEE J. Quantum Electron. **QE**-2, 235 (1966).

[30]F. Aronowitz and W. L. Lim, IEEE J. Quantum Electron. **QE**-13, 338 (1977).

[31]W. W. Chow, J. Gea-Banacloche, L. M. Pedrotti, V. E. Sanders, W. Schleich, and M. O. Scully, Rev. Mod. Phys. **57**, 61 (1985).

[32]V. I. Sardyko and V. N. Severikov, J. Appl. Spectrosc. (USSR) **26**, 592 (1977).

[33]V. N. Lisitsyn and B. I. Troshin, Opt. Spektrosk. **22**, 666 (1967) [Opt. Spectrosc. (USSR) **22**, 363 (1967)].

[34]T. J. Hutchings, J. Winocur, R. H. Durrett, E. D. Jacobs, and W. L. Zingery, Phys. Rev. **152**, 467 (1966).

[35]F. Aronowitz, Appl. Opt. **11**, 405 (1972).

[36]S. Schroter and D. Kuhlke, Opt. Quant. Electron. **13**, 247 (1981); D. Kuhlke, Acta Phys. Pol. A **61**, 547 (1982).

[37]See, for example, C. H. Henry and R. F. Kazarinov, IEEE J. Quantum Electron. QE-**22**, 294 (1986); D. Lenstra, B. H. Verbeek, and A. J. Den Boef, *ibid.* QE-**21**, 674 (1985).

[38]See, for example, G. Simmons, *Differential Equations* (McGraw-Hill, New York, 1972); M. Braun, *Differential Equations and Their Applications* (Springer-Verlag, New York, 1977).

[39]H. Haken, *Synergetics* (Springer-Verlag, New York, 1977).

[40]J. M. Sancho, M. San Miguel, S. L. Katz, and J. D. Gunton, Phys. Rev. A **26**, 1589 (1982).

[41]T. H. Chyba and L. Mandel, in *Coherence and Quantum Optics VI,* edited by L. Mandel and E. Wolf (Plenum, New York, to be published).

[42]W. R. Christian, Ph.D. thesis, University of Rochester, 1987.

[43]See, for example, S. Singh, S. Friberg, and L. Mandel, Phys. Rev. A **27**, 381 (1983); W. R. Christian and L. Mandel, Opt. Commun. **64**, 537 (1987).